

Mechanism of Spontaneous Blebbing Motion of an Oil–Water Interface: Elastic Stress Generated by a Lamellar–Lamellar Transition

Yutaka Sumino,^{*,†} Norifumi L. Yamada,[‡] Michihiro Nagao,^{§,||} Takuya Honda,[⊥] Hiroyuki Kitahata,[#] Yuri B. Melnichenko,[∇] and Hideki Seto[‡]

[†]Department of Applied Physics, Faculty of Science, Tokyo University of Science, Katsushika, Tokyo 125-8585, Japan

[‡]KENS&CMRC, Institute of Materials Structure Science, High Energy Accelerator Research Organization, Tokai, Ibaraki 319-1106, Japan

[§]NIST Center for Neutron Research, National Institute of Standards and Technology, Gaithersburg, Maryland 20899-6102, United States

^{||}Center for Exploration of Energy and Matter, Indiana University, Bloomington, Indiana 47408 United States,

[⊥]Department of Education, Aichi University of Education, Kariya, Aichi 448-8542, Japan

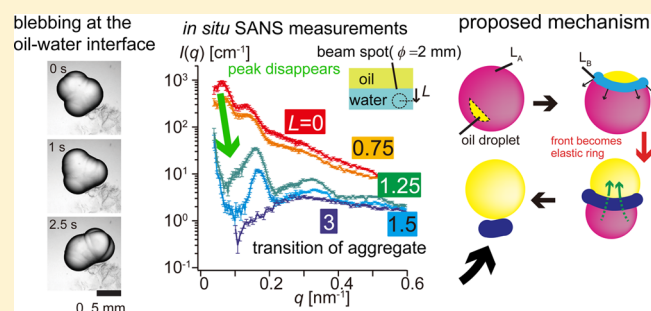
[#]Department of Physics, Graduate School of Science, Chiba University, Chiba, Chiba 263-8522, Japan

[∇]Biology and Soft Matter Division, Oak Ridge National Laboratory, Oak Ridge, Tennessee 37831-6393, United States

W Web-Enhanced Feature **S** Supporting Information

ABSTRACT: A quaternary system composed of surfactant, cosurfactant, oil, and water showing spontaneous motion of the oil–water interface under far-from-equilibrium condition is studied in order to understand nanometer-scale structures and their roles in spontaneous motion. The interfacial motion is characterized by the repetitive extension and retraction of spherical protrusions at the interface, i.e., blebbing motion. During the blebbing motion, elastic aggregates are accumulated, which were characterized as surfactant lamellar structures with mean repeat distances d of 25 to 40 nm. Still unclear is the relationship between the structure formation and the dynamics of the interfacial motion.

In the present study, we find that a new lamellar structure with d larger than 80 nm is formed at the blebbing oil–water interface, while the resultant elastic aggregates, which are the one reported before, have a lamellar structure with smaller d (25 to 40 nm). Such transition of lamellar structures from the larger d to smaller d is induced by a penetration of surfactants from an aqueous phase into the aggregates. We propose a model in which elastic stress generated by the transition drives the blebbing motion at the interface. The present results explain the link between nanometer-scale transition of lamellar structure and millimeter-scale dynamics at an oil–water interface.



INTRODUCTION

A cell generates motion through the conversion of chemical energy into macroscopic mechanical forces. In this process, the coupling of spontaneous symmetry breaking with motion¹ plays crucial role in addition to genetic information. Since physicochemical systems are less complex than biological systems and are more readily reproduced, they represent effective alternatives to the direct analysis of biological systems. As such, various researchers have attempted to mimic biological motility using artificial droplets.^{2,3} Despite these successes, the previously reported physicochemical systems all utilize surface tension as a driving force, such as the Marangoni effect, and are different from cells that use elastic stress^{4–6} to drive their motion. Thus, it would be beneficial to develop physicochemical systems that move spontaneously due to elastic stress.

On this basis, several of the present authors have recently developed an oil–water system in which the interface

spontaneously undergoes interfacial motion. The motion, driven due to elastic stress, is characterized by the repetitive extension and retraction of spherical protrusions at the interface; i.e., blebbing motion.^{7–10} In constructing these experiments, we applied an ionic surfactant/cosurfactant/water system.^{11–15} We prepared a system consisting of stearyltrimethylammonium chloride (STAC, an ionic surfactant) dissolved in water (an aqueous phase) and palmitic acid (PA, a cosurfactant) dissolved in tetradecane (an organic phase). Setting a droplet of the organic phase floating on the aqueous phase, the droplet shows the blebbing motion at an oil–water interface with formation of semitransparent aggregates (Figure 1a).^{8,9} An essential characteristic of the

Received: January 12, 2016

Revised: March 2, 2016

Published: March 3, 2016

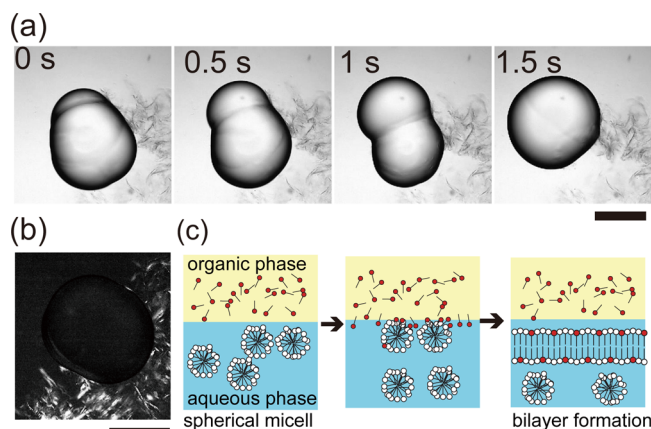


Figure 1. (a,b) Microscope images of interfacial blebbing accompanied by semitransparent aggregate formation, obtained from a $0.5 \mu\text{L}$ oil droplet on an aqueous phase with $C_s = 20 \text{ mmol/L}$: (a) bright field snapshots (see [Movie 1](#)) and (b) polarized crossed Nicols (see [Movie 2](#)) microscope image. The scale bars correspond to 0.5 mm . In panel a, the aggregates were peeled away from the oil–water interface at the constricted part of the interface. An aggregate that had already detached from the oil–water interface was accumulated around the droplet seen in the lower right corner of all images, and shows birefringence as depicted in panel b. (c) Schematics of molecular aspect of aggregate formation. Bars with white (red) circles represent STAC (PA) molecules.

blebbing motion is the absence of global convective patterns inside both the organic and the aqueous phases, which clearly contrasts¹⁶ with the more common Marangoni instability.^{17,18} The molecular aspect of the system in relation with the blebbing motion can be inferred from the fact that the semitransparent aggregates have birefringence. Such birefringence is one of characteristic features of a lamellar structure ([Figure 1b](#)). STAC in the aqueous phase forms spherical micelle, whereas PA is not soluble to water without the presence of STAC. Once the aqueous and the organic phases are in contact, PA molecules in the organic phase are absorbed into the STAC micelles in the aqueous phase. Due to a larger packing parameter¹⁹ of PA (larger than 1) than that of STAC (smaller than $1/3$), the STAC micelles, then, elongate to form bilayers. Thus, the micellar phase turns to the lamellar structure, and the lamellar structure forms semitransparent aggregates ([Figure 1c](#)).^{11–15,20} Recent studies to more closely look at the oil–water interface using small-angle X-ray scattering (SAXS) confirmed that the generated semitransparent aggregates consist of lamellar structures.^{10,21} Based on this result, we have developed a mathematical model⁹ that considers the semitransparent aggregates as a simple elastic gel. This model correctly predicted several experimental observations.

More recent data, however, show an insufficiency of the model as the passive aggregate cannot produce enough pressure for the blebbing motion.²² In addition to that, it is found that the aggregate formation does not necessarily lead to the blebbing motion: the blebbing motion is suppressed when turbid aggregates, instead of semitransparent aggregates, are formed at the oil–water interface under high STAC concentration.⁸ These facts imply that there are missing pieces of information to explain the blebbing motion, such as a difference in nanometer-scale structures in the different form of aggregates and how elastic stress is produced by the aggregates. Therefore, microscopic investigations of the surfactant

aggregates formed at an oil–water interface, as well as their dynamics, are required to clarify the mechanism of the blebbing motions. For this purpose, here we conducted *in situ* small-angle neutron scattering (SANS) and SAXS analyses of the semitransparent and turbid aggregates to elucidate the microscopic factors for the blebbing motion. The data demonstrated that both the semitransparent and turbid aggregates are in the same type of lamellar phase. However, a different type of lamellar phase with large repeat distance is observed at the blebbing interface. These results indicate that the transition of the lamellar phases characterized by shrinkage in the repeat distance plays key roles to have blebbing motion at the oil–water interface and the formation of semitransparent aggregates. Herein we propose possible mechanisms for the interfacial blebbing motion, based on the transition of the lamellar phase and the effect of elastic stress.

EXPERIMENTS

Materials. The oil–water system was composed of an aqueous phase consisting of a D_2O solution of STAC, while an organic phase was a tetradecane ($\text{C}_{14}\text{H}_{30}$) or deuterated tetradecane ($\text{C}_{14}\text{D}_{30}$) solution of PA. Although light water has been used in our previous studies,^{7–10} the present study employed heavy water (D_2O) (99.9%) since the use of a deuterated solvent was necessary to obtain a suitable contrast between the solvent and surfactants in the SANS data. This was done even in real space and SAXS measurements to maintain the same conditions as in the SANS analysis. The concentration of PA in the organic phase was kept constant at 20 mmol/L , whereas that of STAC in the aqueous phases were varied and are denoted herein as C_s . $\text{C}_{14}\text{D}_{30}$ (98% isotope purity) instead of $\text{C}_{14}\text{H}_{30}$ was used for a SANS experiment when it is stated explicitly. All measurements were carried out at an ambient temperature of approximately $22 \text{ }^\circ\text{C}$.

Observation of Interfacial Motion. Optical microscopy (as in [Figure 1a,b](#)) was performed using a polarized microscope equipped with a $\times 5$ objective lens. In these observations, a $3 \mu\text{L}$ aliquot of the aqueous phase in which $C_s = 20 \text{ mmol/L}$ was placed on a glass substrate, followed by the addition of a $0.5 \mu\text{L}$ droplet of the organic phase to the aqueous surface.

Microscope slide was used as a window to construct a vessel for the observation of interfacial motion ([Figure 2a](#)). The thickness, width and height of the vessel were 2 mm , 55 mm and 40 mm , respectively. A 2 mL aliquot of the aqueous phase was transferred into the vessel followed by 1 mL of the organic phase such that this phase was positioned on top of the aqueous phase. The motion of the interface was recorded using the shadowgraph technique and observed using a digital video camera.

The value of C_s was varied from 10 to 60 mmol/L and observations were conducted to assess the blebbing motion. We first confirmed that the appearance of the turbid aggregates always accompanies the suppression of blebbing motion as in the previous study.⁸ Thus, we observed the suppression of interfacial motion for the indication of the turbid aggregates. During these trials, the vessel was loaded with the organic and aqueous phases as described above, and the vessel was allowed to sit for 40 min , following which the presence of turbid aggregates was determined, as shown in [Figures 2c–2](#) and [d–2](#). At least seven independent measurements were conducted at each concentration. From these measurements, a value for the suppression rate of blebbing motion, P , which also corresponds to the appearance rate of turbid aggregate, was obtained.

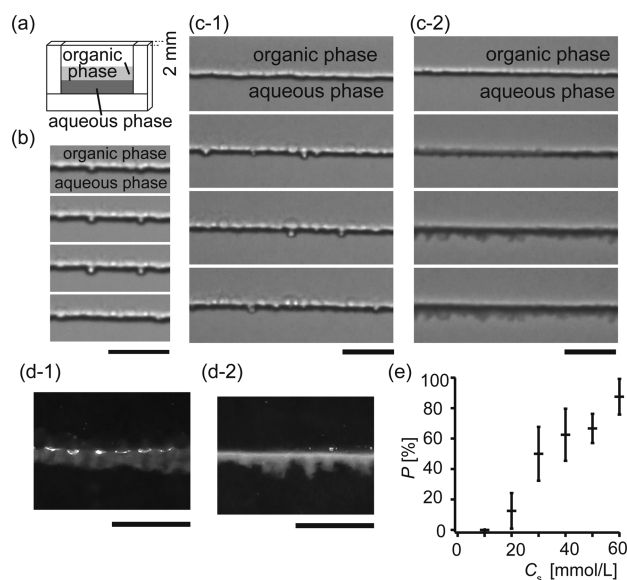


Figure 2. Interfacial blebbing accompanied by aggregate formation. (a) Schematic representation of a typical experimental setup, (b) shadowgraph images of interfacial motion ($C_s = 20$ mmol/L) in which two blebs extend and retract (time step = 0.5 s; see also [Movie 3](#)), (c) shadowgraph images of a blebbing interface ($C_s = 20$ mmol/L, c-1; [Movie 3](#)) and an interface without blebbing due to coverage by turbid aggregates ($C_s = 50$ mmol/L, c-2; [Movie 4](#)) (time step = 200 s), (d) reflection images of aggregates after 1 h, showing a semi-transparent aggregate that appeared when the interface was blebbing ($C_s = 20$ mmol/L, d-1) and a turbid aggregate ($C_s = 50$ mmol/L, d-2), and (e) probability of turbid aggregate appearance, P , is plotted with respect to C_s . Error bars shown in the figures represent \pm one standard deviation of the bimodal distribution. All scale bars correspond to 5 mm.

SANS Analyses. SANS analyses were conducted using the general purpose SANS instrument²³ at the Oak Ridge National Laboratory. The sample–detector distances were chosen to cover a range of scattering vectors, q , from 0.05 nm^{-1} to 0.6 nm^{-1} , where $q = 4\pi\lambda^{-1} \sin \theta$ and 2θ is the scattering angle. The neutron wavelength, λ , was set to 0.6 nm , with a wavelength resolution, $\Delta\lambda/\lambda$, of 0.13 . Scattered neutrons were detected using a $1 \text{ m} \times 1 \text{ m}$ helium-filled two-dimensional (2D) position-sensitive detector with $5 \text{ mm} \times 5 \text{ mm}$ pixel resolution. The raw 2D data were corrected for the detector pixel sensitivity, empty cell scattering and dark current. The 2D SANS patterns were sector-averaged in the directions perpendicular and parallel to the interface to produce a one-dimensional profile: $I(q)$. The beam size at the sample position was 2 mm and the acquisition time for each measurement was 10 min .

Quartz cells with a 2 mm flight path were used in the experimental trials. A $300 \mu\text{L}$ aliquot of the aqueous phase was injected into the cell followed by $150 \mu\text{L}$ of the organic phase. For in situ measurements, the beam was directed at the oil–water interface and scattering data were subsequently obtained. For the spatial scanning measurements, the samples were allowed to mature for 12 h after the organic phase was put into contact with the aqueous phase, and were then scanned from the oil–water interface to the aqueous phase. For the spatial scanning measurements, $C_{14}D_{30}$ was used as solvents in the organic phase to have better signal-to-noise ratio in the SANS data.

SAXS Analyses. SAXS data were acquired using the SAXS instruments at BL6A in the Photon Factory, High Energy Accelerator Research Organization, Tsukuba, Japan. The incident X-rays were monochromatized with Ge(111) and a wavelength, λ , of 0.15 nm was used with a resolution of $\Delta\lambda/\lambda = 0.003$. The scattering data were obtained using a detector for taking an image of $168.7 \text{ mm} \times 179.4 \text{ mm}$ with a resolution of $172 \mu\text{m}$. The beam spot size at a sample vessel was approximately $0.25 \text{ mm} \times 0.5 \text{ mm}$ (height and width), and a vessel with thickness, width and height of 2 mm , 40 mm and 25 mm , respectively, was used, having beam windows made of a polyimide film. The acquisition time for each measurement was 5 s . In these trials, $600 \mu\text{L}$ of the aqueous phase was transferred into the vessel, followed by $300 \mu\text{L}$ of organic phase, placed on top of the aqueous phase. During spatial scanning, the beam spot was moved from the oil–water interface of the sample 2 h after preparation.

RESULTS

Concentration Dependence of Interfacial Motion.

First, we reconfirmed the blebbing motion, whose repetition time was of the order of a second, under various conditions before scattering experiments. As summarized in this section, H_2O to D_2O exchange did not affect the main characteristic features of the system. The typical blebbing motion of a droplet of organic phase floating on the aqueous phase is shown in [Figure 1](#). Since the droplet diameter ($\approx 1 \text{ mm}$) was smaller than the capillary length ($\approx 3 \text{ mm}$), the droplet was assumed to have a spherical shape. The droplet was seen to undergo repeated deformation characterized by a ring-shape constricted part of the oil–water interface ([Figure 1a](#)). At this constricted part, an aggregate generating birefringence peeled away from the oil–water interface. The aggregate then completely detached and was dispersed in the aqueous phase ([Figure 1b](#)). The thickness of these aggregates immediately after release from the oil–water interface was less than 1 pixel, corresponding to $4 \mu\text{m}$. Thus, the thickness of the aggregates is believed to be less than $4 \mu\text{m}$.

This interfacial blebbing was also observed in flat geometry, a quasi 2D system, using the vessel shown in [Figure 2a](#). Following contact between the organic and aqueous phases, the oil–water interface showed blebbing, as exemplified in [Figure 2b](#) and c-1, at a STAC concentration of $C_s = 20 \text{ mmol/L}$. In [Figure 2b](#), two blebs with a typical size of approximately 1 mm were seen to extend in the direction of the aqueous phase for a period of 2 s before retreating within 0.5 s . This type of bleb appeared and disappeared at many locations around the oil–water interface, as shown in [Figure 2c-1](#), for a period of more than 1 h . During this time span, semitransparent aggregates were generated at the oil–water interface, forming a pillar-like structure ([Figure 2d-1](#)).¹⁰ On closer inspection of the blebbing interface in the flat geometry, a constricted portion from which the aggregates were peeled off was observed, just as in the case of the floating droplet.

With increasing the STAC concentration in the aqueous phase, turbid aggregates were generated instead of semi-transparent ones. [Figure 2c-2](#) presents the typical appearance of the turbid aggregates along with the oil–water interface, for a sample with $C_s = 50 \text{ mmol/L}$. [Figure 2c-2](#) shows a shadowgraph image in which the turbid aggregates appear as a darkened region, while [Figure 2d-2](#) presents a reflected image, in which the aggregates appear white. Once the turbid aggregates appeared, they subsequently covered the whole

oil–water interface. The interface, then, stopped blebbing accompanied by the formation of the turbid aggregates. This same behavior has been reported in the case of droplets,⁸ i.e., turbid aggregates suppress the blebbing motion irrespective of the sample geometry.

The turbid aggregates appear to be formed by a nucleation–growth process, requiring a finite degree of perturbation in the early stage when the large concentration difference exists in the system. Due to this reason, the appearance of the turbid aggregates was stochastic. The appearance rate of the turbid aggregates, P , increased with increasing values of C_s , as shown in Figure 2e. At $C_s = 20$ mmol/L, the turbid aggregates rarely appeared, whereas they were common at $C_s = 50$ mmol/L. Thus, during SANS and SAXS analyses, C_s values of 20 mmol/L and 50 mmol/L were used to compare the structures in the semitransparent aggregates that accompanied the blebbing of the oil–water interface and in the turbid aggregates.

Measurements of SANS at the Oil–Water Interface.

SANS data were acquired to elucidate the nature of aggregates, and the time course of the SANS pattern following contact between the organic and the aqueous phases is shown in Figure 3. The elapsed time, T , indicates the time after contact between organic and aqueous phases. During these trials, a 2 mm diameter neutron beam was irradiated to the oil–water interface. Figure 3a,b presents the SANS patterns obtained with semitransparent aggregates at $C_s = 20$ mmol/L and with turbid aggregates at $C_s = 50$ mmol/L. Only in the case with $C_s = 20$ mmol/L did the oil–water interface show blebbing.

In $C_s = 50$ mmol/L, a sample corresponding to turbid aggregates with no blebbing motion (Figure 3b), a set of Bragg peaks representing an isotropically oriented lamellar structure appeared at $T = 10$ min. The ring pattern was maintained over time although the spacing of the rings gradually changed between $T = 10$ and 120 min. By contrast, the pattern in Figure 3a corresponding to semitransparent aggregates at the blebbing interface, showed a superimposed isotropic ring pattern and an anisotropic butterfly like pattern after $T = 10$ min. The butterfly like pattern was perpendicular to the oil–water interface and grew with time, demonstrating that the number of lamellae parallel to the oil–water interface increased with time.

The sector averages of both patterns are provided in Figure 4. These averages were calculated over 40 degree sectors

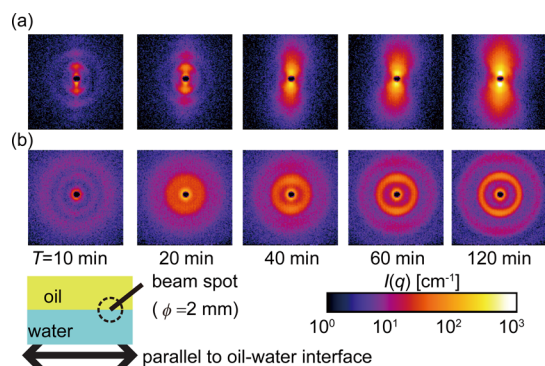


Figure 3. SANS images obtained from (a) semitransparent aggregates at a blebbing interface ($C_s = 20$ mmol/L), and (b) turbid aggregates ($C_s = 50$ mmol/L). T represents elapsed time after contact between the organic and aqueous phases. In series a, anisotropic butterfly like patterns perpendicular to the interface are observed in addition to weak isotropic patterns at small T . The anisotropic scattering grew with time. In series b, the patterns were always isotropic.

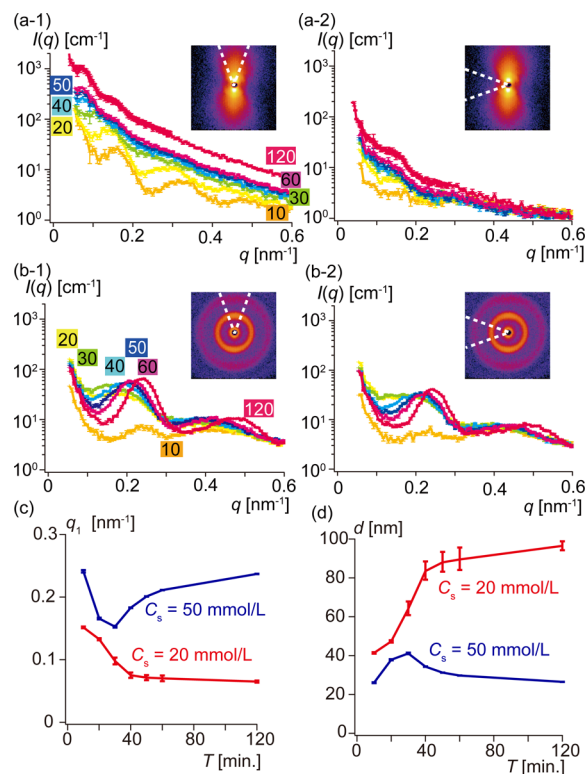


Figure 4. Sector averages of the scattering pattern of (a-1, a-2) semitransparent aggregates at the blebbing interface for which $C_s = 20$ mmol/L and (b-1, b-2) turbid aggregates covering a nonblebbing interface for which $C_s = 50$ mmol/L. The line colors indicate time elapsed after phase contact (T in min: orange = 10, yellow = 20, green = 30, cyan = 40, blue = 50, violet = 60, red = 120). (a-1) and (b-1) correspond to the sectors perpendicular to the oil–water interface, whereas (a-2) and (b-2) correspond to the sectors parallel to the interface. Error bars represent \pm one standard deviation. (c) Position of the first peak, q_1 , obtained by fitting the data in (a-1) and (b-1) to a Gaussian curve. (d) Repeat distances, d , as estimated from $d = 2\pi/q_1$. Error bars represent \pm one standard deviation.

perpendicular (Figure 4a-1 and b-1) and parallel (Figure 4a-2 and b-2) to the oil–water interface. The signals corresponding to the lamellar structure with a set of Bragg peaks were observed in every case. The positions of the first peak, q_1 , were obtained by the fitting these data to a Gaussian function, and the results are plotted in Figure 4c. In the sector average perpendicular to the oil–water interface, the first peak position, q_1 , of the turbid aggregates ($C_s = 50$ mmol/L; Figure 4b-1) slightly shifts to lower q values between 10 and 30 min, then moves to higher q values and reaches a value of $q_1 = (0.2371 \pm 0.0003)$ nm⁻¹ at $T = 120$ min (Figure 4c). Contrary to the turbid aggregates, q_1 obtained from the semitransparent aggregate ($C_s = 20$ mmol/L) in the direction perpendicular to the interface (Figure 4a-1) continually shifted to lower q values and eventually converged on a value of $q_1 = (0.065 \pm 0.002)$ nm⁻¹ at $T = 120$ min (Figure 4c). Estimating the repeat distance from $d = 2\pi/q_1$ (Figure 4d), the lamellar structure in the semitransparent aggregates at the blebbing interface exhibited increased d values with time and reached a value of $d = (96 \pm 2)$ nm. The lamellar structure in the turbid aggregate showed a maximum $d = (41.1 \pm 0.4)$ nm at $T = 30$ min, and then decreasing d values with time to $d = (26.50 \pm 0.03)$ nm. In the case of the semitransparent aggregate at the blebbing interface, the signal in the parallel direction was smaller than

that in the perpendicular, and the peak position at 120 min was in the vicinity of $q = (0.13 \pm 0.03) \text{ nm}^{-1}$, corresponding to $d = (49 \pm 18) \text{ nm}$. The above results are summarized in Table 1.

In the previous SAXS measurements, which were conducted more than 80 min after the contact of the oil–water interface,^{10,21} a typical repeat distance d of lamellar structures was about 44 nm in the case of $C_s = 20 \text{ mmol/L}$, and was 28 to 30 nm in the case of $C_s = 50 \text{ mmol/L}$. In the present SANS measurement, we confirmed the lamellar structure with $d = (49 \pm 18) \text{ nm}$ in the parallel direction at the semitransparent aggregates ($C_s = 20 \text{ mmol/L}$). We also confirmed that $d = (26.50 \pm 0.03) \text{ nm}$ at the turbid aggregate ($C_s = 50 \text{ mmol/L}$). Considering the generated aggregate was not homogeneous, the observed repeat distance d was consistent with the previous SAXS measurement. The comparison with the present and the previous data is summarized in Table 2. In addition to the previously reported lamellar structure, here we found the oriented lamellar structure parallel to the oil–water interface with the repeat distance $d = (96 \pm 2) \text{ nm}$ (Figure 4a-1 and d). Hereafter, we call the newly found lamellar structure with large d as L_A , and the previously reported lamellar structure^{10,21} with small d as L_B . This finding of L_A can be attributed to the experimental geometry, especially in the beam size of SANS (2 mm) and micro beam SAXS used in the previous study (5 μm). In the past study with SAXS, the beam spot was 1 mm below the oil–water interface, and the vicinity of the oil–water interface was not observed. For this reason, we infer that L_A is localized near the oil–water interface.

In order to confirm the position dependence of L_A and L_B , we examined the semitransparent aggregates at the blebbing interface ($C_s = 20 \text{ mmol/L}$) 12 h after preparation. In these observations, we confirmed that the interface continued to exhibit the blebbing motion, although the motion was weaker than that immediately after preparation. The beam position was moved from the interface ($L = 0 \text{ mm}$) into the aqueous phase (up to $L = 3 \text{ mm}$). Figure 5a shows the SANS patterns; the anisotropic patterns at the interface ($L < 1 \text{ mm}$) were visible even 12 h after sample preparation. Surprisingly, a ring pattern similar to that created by the turbid aggregates was seen when the beam spot was in the semitransparent aggregate far from the interface, at $L > 1 \text{ mm}$.

Figure 5b,c shows the signals obtained from sector-averaging perpendicular and parallel to the oil–water interface (the angular range is depicted in Figure 5a as a dashed line). The positions of the first peak, q_1 , were obtained by fitting these data to a Gaussian function, and the results are plotted in

Table 1. Observed Condition of q_1 and d Obtained from Temporal Scan with SANS

condition	q_1 [nm^{-1}]	d [nm]
$C_s = 20 \text{ mmol/L}$		
perpendicular to the interface		
$T = 10 \text{ min}$	0.152 ± 0.001	41.4 ± 0.4
$T = 30 \text{ min}$	0.098 ± 0.005	64 ± 4
$T = 120 \text{ min}$	0.065 ± 0.002	96 ± 2
parallel to the interface		
$T = 120 \text{ min}$	0.13 ± 0.03	49 ± 18
$C_s = 50 \text{ mmol/L}$		
$T = 10 \text{ min}$	0.241 ± 0.002	26.0 ± 0.2
$T = 30 \text{ min}$	0.153 ± 0.001	41.1 ± 0.4
$T = 120 \text{ min}$	0.2371 ± 0.0003	26.50 ± 0.03

Table 2. Comparison of Estimated Repeat Distance of Lamellar Structure in the Aggregate with the Present and the Previous Observation

observation	d ($C_s = 20 \text{ mmol/L}$)		d ($C_s = 50 \text{ mmol/L}$)	
	L_A	L_B	L_B	L_B
present study (SANS)	96 ± 2	49 ± 18	26.50 ± 0.03	L_B
previous study (SAXS ¹⁰)	43.6	L_B	28 to 30	L_B

The data obtained at $T = 120 \text{ min}$ from the perpendicular direction is used for the values in the present study.

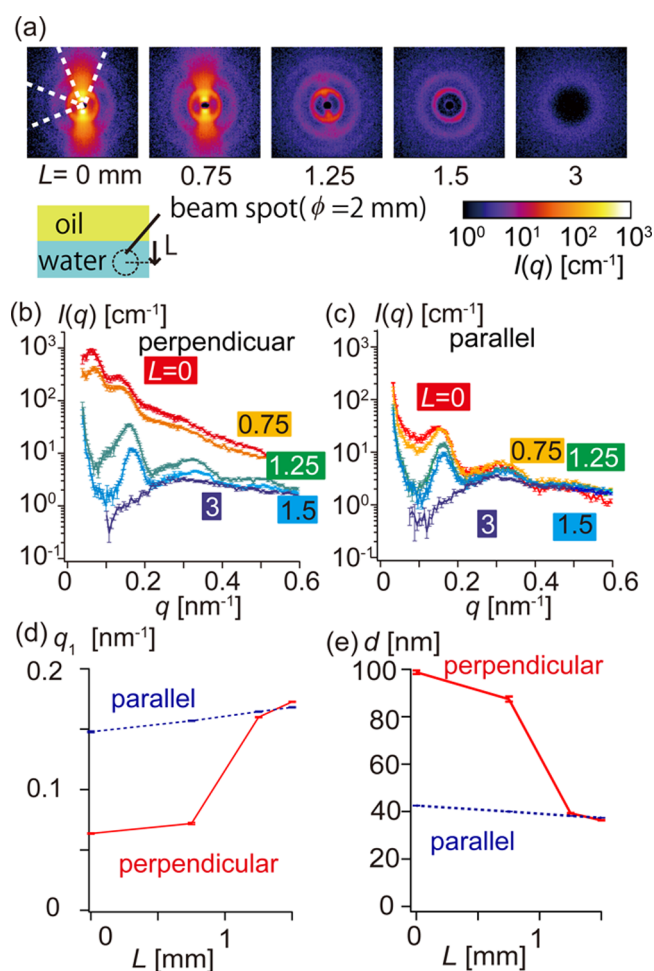


Figure 5. (a) SANS images obtained from the semitransparent aggregate at the blebbing oil–water interface 12 h after the sample preparation ($C_s = 20 \text{ mmol/L}$). L indicates the position of the beam spot relative to the interface. Organic solvent was $\text{C}_{14}\text{D}_{30}$. Signals averaged over sectors (b) perpendicular to and (c) parallel to the oil–water interface indicated in panel a by white dashed lines. The color of the markers with number represents the distance from the oil–water interface, L , in millimeters. (d) Position of the first peak, q_1 , obtained by fitting the data in panels b and c to a Gaussian curve. Red solid and blue dotted curves correspond to the data obtained from perpendicular and parallel sectors, respectively. (e) Repeat distances, d , as estimated from $d = 2\pi/q_1$ with respect to L . Red solid and blue dotted curves correspond to the data obtained from perpendicular and parallel sectors, respectively. The lamellae with large d values appeared only in the perpendicular sectors and disappeared when the beam spot deviated from the oil–water interface ($L \approx 1 \text{ mm}$; dotted line). Error bars representing \pm one standard deviation are also shown, but they are not visible as they are too small in this plot.

Figure 5d. Notably small q_1 were observed only from the average over perpendicular sector at $L < 1$ mm. The mean repeat distances of the lamellae, d , obtained from the first peak position, q_1 , are shown in Figure 5e. When the 2 mm neutron beam was positioned at the oil–water interface, L_A , the lamellar structure was characterized by large d and anisotropic pattern was observed. This is in good agreement with the data obtained from dynamic measurements of semitransparent aggregates exactly at the blebbing oil–water interface (Figure 4a). At $L > 1$ mm, L_B , the lamellar structure characterized by smaller d was observed. The isotropic pattern shown in Figure 5a also supports that the nanometer scale structure of the semitransparent aggregates for large L was L_B , which is the same as those found in the turbid aggregates. Therefore, it was confirmed that L_B was observed in both $C_s = 20$ mmol/L (semitransparent aggregates) and 50 mmol/L (turbid aggregates). The difference in the macroscopic appearance of these aggregates was attributed to a long wavelength structure (larger than μm) but not to the microscopic lamellar structure. In addition, we found that L_A existed in the proximity of the oil–water interface only in the case of $C_s = 20$ mmol/L (Table 3). These findings lead to our conclusion that the semitransparent aggregates are formed out of the transition from L_A to L_B .

Measurements of SAXS at the Oil–Water Interface.

The SANS data at the blebbing oil–water interface demonstrated that the transition of the lamellar structure from L_A to L_B was characterized by a reduction of d . Unfortunately, the large diameter of the neutron beam (2 mm) and long exposure time (10 min) used for SANS measurements made it difficult to determine the spatial and temporal distributions of d with respect to L . To resolve this problem, SAXS analyses were performed using a much smaller beam size (0.25 mm \times 0.5 mm) and shorter exposure time (5 s).

Data were acquired 2 h after setting the organic phase on the aqueous phase, using a sample of $C_s = 20$ mmol/L. Figure 6 presents typical SAXS results obtained in the semitransparent aggregates. The one shown in Figure 6a was obtained at the oil–water interface, whereas the one shown in Figure 6b was obtained at $L = 2.5$ mm below the interface. The first and second peaks in Figure 6a were located at (0.071 ± 0.003) nm^{-1} and (0.148 ± 0.007) nm^{-1} , and originated from a lamellar structure with $d = (89 \pm 4)$ nm. The peak appeared in the perpendicular direction relative to the oil–water interface. By contrast, the pattern becomes more complex and less polarized when moving away from the oil–water interface. As seen in Figure 6b, two distinctive signals were generated, corresponding to two different domains. Taking the sector averages

Table 3. Comparison of Types of Lamellar Observed for Different Position L and Concentration C_s

condition	d [nm]	type of lamellar
$C_s = 20$ mmol/L	Semitransparent Aggregate	
$L = 0$ mm	98.8 ± 0.7	L_A
$L = 1.5$ mm	36.39 ± 0.07	L_B
$C_s = 50$ mmol/L ^a	Turbid Aggregate	
$L = 0$ min	26.50 ± 0.03	L_B

L_B was observed in the both types of aggregates, but L_A was observed only when semitransparent aggregates were found. ^aThe data from Figure 4 at $T = 120$ min are used for the data of $C_s = 50$ mmol/L at $L = 0$.

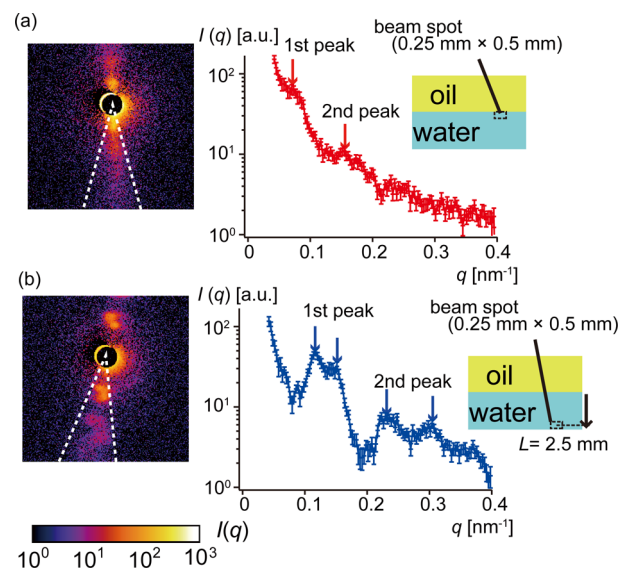


Figure 6. Observed SAXS patterns and the sector averages obtained (a) almost at the oil–water interface and (b) 2.5 mm below the interface. Here the oil–water interface was blebbing for both cases, and $C_s = 20$ mmol/L. In panel a the first and the second peaks were located at (0.071 ± 0.003) nm^{-1} and (0.148 ± 0.007) nm^{-1} , which correspond to $d = (89 \pm 4)$ nm. In panel b, there appeared four distinctive peaks. Two of them are (0.118 ± 0.001) nm^{-1} , and (0.237 ± 0.001) nm^{-1} , corresponding to $d = (53.5 \pm 0.5)$ nm. The rest of them are (0.144 ± 0.002) nm^{-1} , and (0.298 ± 0.002) nm^{-1} , corresponding to $d = (43.6 \pm 0.7)$ nm. Considering these signals come from different angles in the scattering pattern, these lamellar structures with different d correspond to different domains. Error bars shown in the figures represent \pm one standard deviation.

generated four distinct peaks at (0.118 ± 0.001) nm^{-1} , (0.144 ± 0.002) nm^{-1} , (0.237 ± 0.001) nm^{-1} , and (0.298 ± 0.002) nm^{-1} , corresponding to lamellar structures for which $d = (43.6 \pm 0.7)$ nm and (53.5 ± 0.5) nm. It should be noted that a similar SAXS pattern for which d was approximately 40 nm was already reported at $L = 1$ mm below the interface.^{10,21}

In summary, these results confirmed that L_A , with oriented lamellar structures with a large d value, was present in the semitransparent aggregate only at the blebbing oil–water interface. In the semitransparent aggregates at $L = 2.5$ mm below the interface, the SAXS detected anisotropic pattern from two different domains of lamellar structure. The difference of these patterns from the symmetric ring pattern detected with the SANS is due to the difference in the beam size and exposure time. The beam size and exposure time of the SAXS are 4% and 0.8% of those of SANS, respectively; hence, the pattern obtained in SANS was an average from different domains over time and showed a symmetric ring pattern.

DISCUSSION

The Relation between L and the Time after Aggregates Were Formed. Here we would like to clarify the relation between L and the time after semitransparent aggregates were formed. While the interface was ($C_s = 20$ mmol/L), the aggregate was peeled off from the oil–water interface, and they formed the pillar-like structure. These pillars grew approximately 1.5 mm in 2 h, and then the length gradually saturated at less than 2 mm.¹⁰ From the fact that the shape of the end part of a pillar did not change during the growth, we anticipate that the aggregate in the pillar was

pushed downward by the newly formed aggregate. In this way, the position of the aggregate, the distance from the oil–water interface L , is connected with the time after aggregates were formed at the oil–water interface. In other words, the newly formed lamellar structure was observed only at a small value of L , where we observed L_A . This indicates that L_A is fresh lamellae, and a transition to L_B occurs on the detachment from the oil–water interface. Indeed, the result of SAXS (Figure 6) confirmed that the aggregates detached from the oil–water interface was L_B . Considering the fact that the time-scale of the detachment of aggregates is the same as that of the blebbing motion (~ 1 s), we infer that the time-scale of the transition from L_A to L_B is less than a second.

The Types of Lamellar Structures: L_A and L_B . The interface exhibits a blebbing motion and produces semi-transparent aggregates at $C_s = 20$ mmol/L. In this situation, the SANS and SAXS results suggest that L_A , a lamellar structure having a large value of d (larger than 80 nm) and oriented parallel to the interface, undergoes a transition to L_B , a less oriented lamellar structure in which d is reduced by approximately half of the original (≈ 40 nm). L_B , with $d \approx 25$ nm, is also found in the turbid aggregates ($C_s = 50$ mmol/L) (Figure 3b).

For molecular aspect of the system, we assume that the stability of L_A and L_B is governed by the ratio between STAC and PA: L_A is stable at small φ_s , and L_B is stable at large φ_s , where φ_s denotes a volume fraction of STAC within a bilayer composing the lamellar structure. φ_s increases as the concentration of STAC (PA) increases (decreases) near a bilayer. We should note that there is a continuous supply of STAC molecules from the micelles in the aqueous phase to a bilayer. On the contrary the supply of PA molecules from the organic phase is geometrically restricted only near the oil–water interface. For these reasons, it is reasonable to assume that φ_s increases with time and, hence, with distance from the interface L . Under this assumption, we consider the differences between the semitransparent aggregate at the blebbing interface ($C_s = 20$ mmol/L; Figure 2c-1) and the turbid aggregates ($C_s = 50$ mmol/L; Figure 2c-2) as follows: At the blebbing interface ($C_s = 20$ mmol/L), L_A is thermodynamically stable due to small fraction of STAC (small φ_s), while it becomes metastable deeper into the aqueous phase due to the supply of STAC (increase in φ_s): i.e., L_B is stable in the aqueous phase instead of L_A . Thus, L_A is formed at the interface, and, subsequently, a structural transition to L_B is induced with accumulation of semitransparent aggregates (Figure 7a). By contrast, L_B is thermodynamically stable even at the oil–water interface when the turbid aggregate is formed ($C_s = 50$ mmol/L) since the STAC concentration is high enough (φ_s is too large for stabilizing L_A). Considering the loss of the blebbing motion in this situation, we conclude that the formation of L_A and the structural transition from L_A to L_B are necessary to the interfacial blebbing motion.

The transition of lamellar structure and the interfacial blebbing mechanism. The present results of SANS and SAXS analyses suggest that a transition of the lamellar structure from L_A to L_B is associated with blebbing at the interface. Thus, we further speculate the relationship between the transition and the blebbing motion.

The blebbing motion is characterized by the appearance of a constricted region at the oil–water interface (Figure 1a) and peeling away of aggregates (Figure 1b). The constricted region propagates along the interface until it reaches the end of the

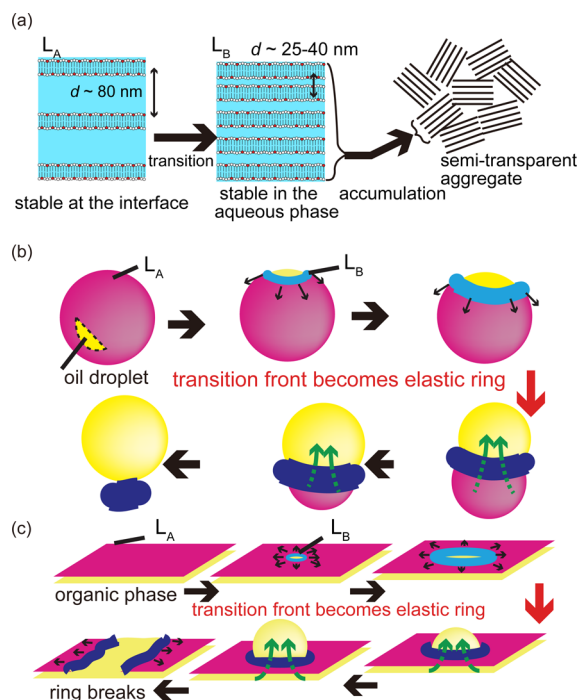


Figure 7. (a) Schematics showing the transition from L_A to L_B and semitransparent aggregate formation in the case of $C_s = 20$ mmol/L. L_A is stable only at the interface, and L_B , instead of L_A , is stable in the other area of the aqueous phase. L_B is then accumulated to be semitransparent aggregate. (b,c) Schematic representations of the lamellar transition and blebbing at the oil–water interface for (b) a droplet and (c) a flat interface. Yellow, pink and blue represent the organic phase, L_A and L_B , respectively. Initially, organic phase (yellow) is covered by L_A (pink sheet). The L_A to L_B transition front (light blue) freely expands at low values of the local density of L_B within the semitransparent aggregate, σ . Once σ exceeds a critical value, σ_c , the semitransparent aggregate at the transition front forms an elastic ring (dark blue) and cannot further expand. Instead, the oil–water interface is drawn into the elastic ring to continue the transition. This process is maintained until the ring (b) detaches from the droplet or (c) is broken.

droplet, at which point the aggregates detach from the interface and drifts into the aqueous phase.

From the SAXS and SANS observations, it appears that the L_A phase is continuously formed at the oil–water interface. As discussed above, L_A is thermodynamically stable at the blebbing interface, but metastable in the aqueous phase, leading to a transition from L_A to L_B in the aqueous phase. Based on this, a mechanism for the blebbing phenomenon is depicted schematically in Figure 7b. Here, we consider the formation of L_A is fast enough and the local concentration at the aqueous phase adjacent to the oil–water interface is always in a steady value (represented by the pink region in this figure). At a certain point, the L_A in the aqueous phase starts transition to L_B (light and dark blue), and the transition front propagates adjacent to the oil–water interface (black arrow). The L_B is simultaneously peeled off and accumulates to produce semitransparent aggregates, whose local density is denoted by σ . The value of σ increases as the transition front propagates. When σ is smaller than a critical value, σ_c , the propagating front freely moves at the interface (light blue) because the front is not elastic enough to restrict this movement. The peeled-off aggregates composed of L_B take on more elastic characteristics when σ exceeds σ_c ; the transition front behaves as an elastic ring (dark blue). The

transition from L_A to L_B should proceed even after the transition front becomes an elastic ring. The front eventually stops expanding, following which the oil–water interface is instead drawn into the elastic ring (green arrow). In this manner, the constricted part is generated, resulting in the formation of a bleb. This process continues until the entire droplet moves out the elastic ring.

In the case of a flat interface, the same concept shown in Figure 7c applies. Here the organic phase is again drawn into the elastic ring, generating a bleb. The difference from the droplet case is the manner in which the bleb disappears. In this case, the bleb disappears when the elastic ring breaks due to the Laplace pressure difference. The same mechanism applies in the case of large droplets, in which breakage of the ring occurs rather than detachment of the ring.^{7,8}

The above scenario explains experimental observation consistently. For example, our previous experiment showed that the smaller bleb size is observed for the higher STAC concentrations.⁷ An increase rate of the density of L_B , σ , with time should be positively correlated with the L_A density on the interface and, hence, L_A formation rate. Thus, σ will be equal to σ_c sooner at higher STAC concentrations, resulting in smaller bleb size. Although further development of the model is required for constructing quantitative discussion, we believe that the present findings take one more step closer to clarifying the nature of the blebbing motion.

Other Possible Mechanisms for Blebbing and Future Study. The sharp change of the repeat distance, d , at the transition from L_A to L_B suggests that the transition is discontinuous. Here, we compare estimated pressure induced by the transition with the required pressure for blebbing motion by assuming that the aggregate macroscopically shrinks to be half in the tangential direction of the oil–water interface due to the decrease in d on the transition. The generated stress by this shrinkage is obtained by the strain multiplied by the Young's modulus of the aggregate B . As the strain is of the order of 1, the tangential stress is the same order as B . The pressure normal to the oil–water interface can be obtained by the tangential stress times the curvature and the thickness of the aggregate h . The additional stress generated by the aggregate is, hence, Bh/r , where r is the radius of the droplet. To have this pressure comparable to the Laplace pressure γ/r due to interfacial tension γ , h must be on the order of $10 \mu\text{m}$.²⁴ This is close to the value obtained from optical measurement ($\sim 4 \mu\text{m}$).

In order to verify the above scenario, we need to confirm that the transition from L_A to L_B is indeed discontinuous. For this purpose, more detailed studies in phase behavior of L_A and L_B as a function of C_s will be relevant. Furthermore, the careful analyses on the response of the macroscopic shape of the aggregates to the reduction of the repeat distance would help in understanding the generation mechanisms of elastic stress. These investigations require further systematic experiments and are left as future studies.

CONCLUSIONS

The present study has reconfirmed first that high surfactant concentrations in an aqueous phase lead to the formation of turbid aggregates and suppression of the blebbing motion, whereas semitransparent aggregates are formed at the blebbing interface. In situ SANS analyses of the oil–water interface, a technique that is able to detect structures averaged over mm-scale and hundreds of seconds during the blebbing,

demonstrated the presence of a lamellar structure, L_B , with a repeat distance ranging from 25 to 40 nm, in both semitransparent and turbid aggregate some distance from the interface. More importantly, a lamellar structure, L_A , with a larger repeat distance (larger than 80 nm), was observed in the semitransparent aggregates only at the blebbing interface. Utilizing SAXS measurements with better spatial and temporal resolution of the beam spot, the above results obtained from the SANS measurements were also supported. The results suggest that the L_A transitions into an L_B soon after it departs from the interface, and this transition is essential for the blebbing motion and formation of semitransparent aggregates.

Based on these experimental results, we believe that the blebbing motion is caused by propagation of the transition front from L_A to L_B adjacent to the oil–water interface. An essential aspect of this mechanism is that the front behaves as an elastic ring when the local concentration of accumulated semitransparent aggregates composed of L_B exceeds a critical value.

The above hypothetical mechanism successfully explains many of our experimental observations. In order to verify the hypothesis, we are currently trying to produce equilibrium phase diagram of STAC/PA/water to confirm the assumption that the stability of L_A and L_B is controlled by the ratio ϕ_s . Furthermore, the experimental estimation of σ and developing a mathematical model based upon our hypothesis will support our quantitative understanding of the blebbing mechanisms proposed here.

The present study shows that a simple physicochemical system composed of oil, water, and surfactants can behave as a type of gel that generates elastic stress by itself. Formerly, such gels have been found only in biological materials.^{25–27} Using our purely physicochemical systems, experiments can be performed with comparative ease, low cost, and better reproducibility compared with trials employing biological materials.

ASSOCIATED CONTENT

Supporting Information

The Supporting Information is available free of charge on the ACS Publications website at DOI: 10.1021/acs.langmuir.6b00107.

Descriptions of the movies (PDF)

Web-Enhanced Feature

WEOs are available in the HTML version of the paper for Figures 1a,b and 2b,c-1,c-2.

AUTHOR INFORMATION

Corresponding Author

*Tel/Fax: +81-3-5876-1393; electronic address: ysumino@rs.tus.ac.jp.

Author Contributions

The manuscript was written through contributions of all authors. All authors have given approval to the final version of the manuscript.

Notes

The authors declare no competing financial interest.

ACKNOWLEDGMENTS

This work was supported in part by a Grant-in-Aid for Young Scientists B by JSPS to Y.S. (No. 24740287) and by the U.S.–

Japan Cooperative Program on Neutron Scattering, and also performed under the Cooperative Research Program of "Network Joint Research Center for Materials and Devices." M.N. acknowledges the funding support of cooperative agreement 70NANB10H255 from NIST, U.S. Department of Commerce. The authors wish to thank M. Hishida (University of Tsukuba) for helpful discussions. The SAXS analyses were performed under the approval of the Photon Factory Program Advisory Committee (Proposal Nos. 2013G530 and 2013G525). The authors also extend special thanks to N. Igarashi and N. Shimizu (Photon Factory, KEK) for their invaluable assistance in obtaining data from beamline BL6A. The SANS analyses were performed under the approval of the HFIR (Cycle 445 CG-2; IPTS-7094). The research at Oak Ridge National Laboratory's High Flux Isotope Reactor was sponsored by the Scientific User Facilities Division, office of Basic Energy Sciences, U.S. Department of Energy.

REFERENCES

- (1) Kozlov, M. M.; Mogilner, A. Model of Polarization and Bistability of Cell Fragments. *Biophys. J.* **2007**, *93*, 3811–3819.
- (2) Hanczyc, M. M.; Toyota, T.; Ikegami, T.; Packard, N.; Sugawara, T. Fatty Acid Chemistry at the Oil-Water Interface: Self-Propelled Oil Droplets. *J. Am. Chem. Soc.* **2007**, *129*, 9386–9391.
- (3) Thutupalli, S.; Seemann, R.; Herminghaus, S. Swarming behavior of simple model squirmers. *New J. Phys.* **2011**, *13* (7), 073021.
- (4) Alberts, B.; Johnson, A.; Lewis, J.; Raff, M.; Roberts, K.; Walter, P. *Molecular Biology of Cells*, 5th ed.; Garland Science: New York, 2007.
- (5) Kruse, K.; Joanny, J. F.; Jülicher, F.; Prost, J.; Sekimoto, K. Asters, Vortices, and Rotating Spirals in Active Gels of Polar Filaments. *Phys. Rev. Lett.* **2004**, *92*, 078101.
- (6) Salbreux, G.; Joanny, J. F.; Prost, J.; Pullarkat, P. Shape oscillations of non-adhering fibroblast cells. *Phys. Biol.* **2007**, *4*, 268–284.
- (7) Sumino, Y.; Kitahata, H.; Seto, H.; Yoshikawa, K. Blebbing dynamics in an oil-water-surfactant system through the generation and destruction of a gel-like structure. *Phys. Rev. E* **2007**, *76*, 055202.
- (8) Sumino, Y.; Kitahata, H.; Seto, H.; Nakata, S.; Yoshikawa, K. Spontaneous Deformation of an Oil Droplet Induced by the Cooperative Transport of Cationic and Anionic Surfactants through the Interface. *J. Phys. Chem. B* **2009**, *113*, 15709–15714.
- (9) Sumino, Y.; Kitahata, H.; Seto, H.; Yoshikawa, K. Dynamical blebbing at a droplet interface driven by instability in elastic stress: a novel self-motile system. *Soft Matter* **2011**, *7*, 3204–3212.
- (10) Sumino, Y.; Kitahata, H.; Shinohara, Y.; Yamada, N. L.; Seto, H. Formation of a Multiscale Aggregate Structure through Spontaneous Blebbing of an Interface. *Langmuir* **2012**, *28*, 3378–3384.
- (11) Yamaguchi, M.; Noda, A. Structures of the Associates Formed in the Ternary System Composed of 1-Hexadecanol, Octadecyltrimethylammonium Chloride and Water. *Nippon Kagaku Kaishi* **1989**, 26–32.
- (12) Ho, C. C.; Goetz, R. J.; El-Aasser, M. S.; Vanderhoff, J. W.; Fowkes, F. M. Optical microscopy of lyotropic mesophases in dilute solutions of sodium lauryl sulfate-lauryl alcohol (or cetyl alcohol)-water systems. *Langmuir* **1991**, *7*, 56–61.
- (13) Yamagata, Y.; Senna, M. Change in the two-step flow behavior on aging the ternary mixture comprising monoalkyl cationic surfactant, long-chain alcohol and water I. Viscous flow preceded by incipient elastic deformation. *Colloids Surf., A* **1998**, *132*, 251–256.
- (14) Yamagata, Y.; Senna, M. Change in Viscoelastic Behaviors Due to Phase Transition of the Assembly Comprising Cetyltrimethylammonium Chloride/Cetyl Alcohol/Water. *Langmuir* **1999**, *15*, 4388–4391.
- (15) Yamagata, Y.; Senna, M. Effect of Temperature on the Development of the Internal Structure of the Cetyltrimethylammonium Chloride/Cetyl Alcohol/Water System. *Langmuir* **1999**, *15*, 7461–7463.
- (16) In Marangoni instability, convection drives interfacial deformation. The convective flow is generated due to shear stress on a free interface proportional to the interfacial tension (Marangoni stress). An essential difference from the interfacial motion driven by elastic stress is the presence of convective flow, which is much faster than the interfacial motion.
- (17) Dupeyrat, M.; Nakache, E. Direct Conversion of Chemical Energy Into Mechanical Energy at an Oil Water Interface. *Bioelectrochem. Bioenerg.* **1978**, *5*, 134–141.
- (18) Rednikov, A. Ye.; Ryazantsev, Yu. S.; Velárde, M. G. Drop motion with surfactant transfer in a homogeneous surrounding. *Phys. Fluids* **1994**, *6*, 451–468.
- (19) Israelachvili, J. N.; *Intermolecular and Surface Forces*, 3rd ed.; Academic Press: London, 2011.
- (20) Mixing an ionic surfactant and a cosurfactant with water leads to a formation of surfactant aggregates composed of a lamellar structures.^{11–15} For a cosurfactant, a long chain alcohol or a long chain fatty acid can be used. These systems are applied as emulsion stabilizers in cosmetics since they have both high viscosity and elasticity even at high water contents above 90%.
- (21) The experimental conditions in ref 10 were almost the same as those in the present experiment except that (i) the scanning position was 1 mm below the interface, (ii) the size of beam was approximately 5 μm , (iii) the measurement was conducted at least 80 min after the contact of the organic and the aqueous phases, and (iv) H_2O instead of D_2O was used. The repeat distance of lamellar structure in H_2O was about 44 nm in the case of $C_s = 20$ mmol/L, whereas it was 28–30 nm in the case of $C_s = 50$ mmol/L.
- (22) Blebbing motion was suppressed by interfacial tension, which can be estimated by the Laplace pressure with γ/r where r is droplet radius, and γ is the oil–water interfacial tension. The increased pressure due to aggregate formation can be estimated to be Bh^2/r^2 , as shown in ref 9, where B and h correspond to Young's modulus and thickness of aggregate, respectively. Therefore, a required thickness of aggregate for blebbing, h , can be represented as $h \sim \gamma r/B$. Putting typical values of $r \approx 10^{-2}$ m, $\gamma \approx 10^{-2}$ N/m, and $B \approx 10^3$ Pa¹⁴, yields the required thickness of 0.1 mm. From the optical microscopic measurements (Figure 1), the aggregate thickness at the oil–water interface is less than 1 pixel in the image corresponding to 4 μm , which differs from the theoretical estimation. Therefore, within this framework of discussion, the increased pressure is too small to produce blebbing.
- (23) Wignall, G. D.; Littrell, K. C.; Heller, W. T.; Melnichenko, Y. B.; Bailey, K. C.; Lynn, G. W.; Myles, D. A.; Urban, V. S.; Buchanan, M. V.; Selby, D. L.; Butler, P. D. The 40 m general purpose small-angle neutron scattering instrument at Oak Ridge National Laboratory. *J. Appl. Crystallogr.* **2012**, *45*, 990–998.
- (24) We used the same typical values as ref 22, where $\gamma \approx 10^{-2}$ N/m, and $B \approx 10^3$ Pa¹⁴.
- (25) Mizuno, D.; Tardin, C.; Schmidt, C. F.; MacKintosh, F. C. Nonequilibrium Mechanics of Active Cytoskeletal Networks. *Science* **2007**, *315*, 370–373.
- (26) Nedelec, F. J.; Surrey, T.; Maggs, A. C.; Leibler, S. Self-organization of microtubules and motors. *Nature* **1997**, *389*, 305–308.
- (27) Nishigami, Y.; Ichikawa, M.; Kazama, T.; Kobayashi, R.; Shimmen, T.; Yoshikawa, K.; Sonobe, S. Reconstruction of Active Regular Motion in Amoeba Extract: Dynamic Cooperation between Sol and Gel States. *PLoS One* **2013**, *8*, e70317.